NJC

Accepted Manuscript

Volume 40 | Number 1 | January 2016 | Pages 1–846

NJC

New Journal of Chemistry
www.rsc.org/njc

A journal for new directions in chemistry

ISSN 1144-0546

ROYAL SOCIETY
OF CHEMISTRY

PAPER
Jason B. Benedict et al
The role of atropisomers on the photo-reactivity and fatigue of diarylethene-based metal–organic frameworks

cnrs

This is an Accepted Manuscript, which has been through the Royal Society of Chemistry peer review process and has been accepted for publication.

Accepted Manuscripts are published online shortly after acceptance, before technical editing, formatting and proof reading. Using this free service, authors can make their results available to the community, in citable form, before we publish the edited article. We will replace this Accepted Manuscript with the edited and formatted Advance Article as soon as it is available.

You can find more information about Accepted Manuscripts in the author guidelines.

ROYAL SOCIETY
OF CHEMISTRY

rsc.li/njc

New Journal of Chemistry Accepted Manuscript

Mechanism of Generation of *closo*-Decaborato Amidrazones. Intramolecular Non-covalent B–H••π(Ph) Interaction Determines Stabilization of the Configuration around the Amidrazone C=N Bond

Valeria K. Burianova,[1] Dmitrii S. Bolotin,*[1] Alexander S. Mikherdov,[1] Alexander S. Novikov,[1] Pennie Petrus Mokolokolo,[2] Andreas Roodt,*[2] Vadim P. Boyarskiy,[1] Dmitry Dar'in,[1] Mikhail Krasavin,[1] Vitalii V. Suslonov,[3] Andrey P. Zhdanov,[4] Konstantin Yu. Zhizhin,[4] and Nikolay T. Kuznetsov[4]

[1]Institute of Chemistry, Saint Petersburg State University, Universitetskaya Nab., 7/9, Saint Petersburg 199034, Russian Federation

[2]Department of Chemistry, University of the Free State, P.O. Box 339, Bloemfontein 9300, South Africa

[3]Center for X-ray Diffraction Studies, Saint Petersburg State University, Universitetskii Pr., 26, Saint Petersburg 198504, Russian Federation

[4]N. S. Kurnakov Institute of General and Inorganic Chemistry of the Russian Academy of Sciences, Leninsky Pr., 31, Moscow 119991, Russian Federation

Abstract

Three types of N(H)-nucleophiles, viz. hydrazine, acetyl hydrazide, and a set of hydrazones, were used to study the nucleophilic addition to the C≡N group of the 2-propanenitrilium *closo*-decaborate cluster $(Ph_3PCH_2Ph)[B_{10}H_9NCEt]$, giving *N-closo*-decaborato amidrazones. A systematic mechanistic study of the nucleophilic addition is provided and included detailed synthetic, crystallographic, computational and kinetic work. As a result, two possible mechanisms have been proposed, which consist of firstly a consecutive incorporation of two Nu(H) nucleophiles, with the second responsible for a subsequent rapid proton exchange. The second possible mechanism assumes a pre-formation of a dinuclear $[Nu(H)]_2$ species which subsequently proceeds with the

nucleophilic attack on the boron cluster. The activation parameters for hydrazones indicate a small dependence on bond formation [$\Delta H^{\neq}$ = 6.8–15 kJ·mol^{-1}], but significantly negative entropies of activation [$\Delta S^{\neq}$ ranges from –139 to –164 J·K^{-1}·mol^{-1}] with the latter contributing some 70–80% of the total Gibbs free energy of activation, $\Delta G^{\neq}$. In the X-ray structure of (Z)-(Ph$_3$PCH$_2$Ph)[B$_{10}$H$_9$N(H)=C(Et)NHN=CPh$_2$], very rare intramolecular non-covalent interactions B–H•••π(Ph) were detected and studied by DFT calculations (M06-2X/6-311++G** level of theory) and topological analysis of the electron density distribution within the framework of Bader's theory (QTAIM method). Estimated strength of these non-covalent interactions is 0.8–1.4 kcal/mol.

Introduction

Polyhedral borane clusters have been a subject of significant attention for the past 15 years due to their broad utility in inorganic[1] and coordination chemistry,[2] and also in pharmacology, where they are generally applied as active species for potential boron neutron-capture cancer therapy[3] and as inhibitors of platelet aggregation,[3g] antiviral agents,[4] and modulators of important hormone receptors.[3g] Although *closo*-dodecaborate and relevant carboranes have been extensively studied, the chemistry of a lighter congener, viz. *closo*-decaborate, has received significantly less attention.

The *closo*-decaborate cluster is generally involved in two types of reactions, for example as (*i*) redox transformations of the cluster (reduction to the *nido*-decaborane B$_{10}$H$_{14}$ or 6-substituted *nido*-boranes B$_{10}$H$_{13}$X (where X is OH, F, Cl, Br, or I)[5] or oxidative dimerization leading to [B$_{20}$H$_{18}$]$^{4-}$)[6] and (*ii*) side-chain reactions, viz. substitution of one or two hydrides by a variety of *C*-,[7] *O*-[8] or *N*[7, 9]-nucleophilic species, including nitriles RC≡N.[9] The nitrilium *closo*-decaborates are very easily functionalizable species by nucleophilic addition and 1,3-dipolar cycloaddition respectively, due to the availability of a highly activated C≡N moiety. This nitrile easily reacts with a spectrum of *C*-,[10] *N*-[11] and *O*-nucleophiles,[12] and also with nitrones[13] and azides.[14]

The nucleophilic addition of simple amines RNH_2 (R = Alk, Ar) and Alk_2NH to the $C\equiv N$ group is known for *closo*-decaborate-,[11] *nido*-decaborane-,[15] and cobalt(III) bis(1,2-dicarbollide)[16]-bound nitriles, however, the reactions of nitrilium boron clusters with hydrazine and its derivatives have not been studied previously. Based on this, we chose three types of N(H)-nucleophiles, viz. hydrazine, acetyl hydrazide, and a set of hydrazones to study their nucleophilic addition to the 2-propanenitrilium *closo*-decaborate cluster giving *N-closo*-decaborato amidrazones. Driven by the success of our synthetic experiments and high selectivity of these reactions, we undertook a systematic mechanistic study of the addition. This included detailed kinetic work, and as a result, we obtained a range of nucleophilicity for the N(H)-nucleophiles that includes a wide-ranging variation of their structural types. Diverse analogous reactions involving nucleophilic addition of amines to unsaturated species have been reported earlier.[17] These reactions serve as reference for our mechanistic interpretation of the process, which we conclude from the detailed kinetic study reported herein.

Results and Discussion

Addition of N(H)-nucleophiles to 2-Propanenitrilium *closo*-Decaborate. As the starting materials for the study of the addition of N(H)-nucleophiles to 2-propanenitrilium *closo*-decaborate $(Ph_3PCH_2Ph)[\mathbf{1}]$ (**Scheme 2**), we addressed three types of N-donors, viz. hydrazine (**2a**; **Scheme 1**), acetyl hydrazide (**2b**), and hydrazones (**2c–g**).

NOS	R^2	R^3
2c	NH_2	MeO
2d	NH_2	H
2e	NH_2	Br
2f	NH_2	CF_3
2g	Ph	H
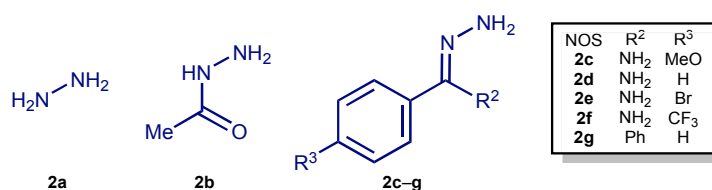
Scheme 1. Structures of three types of the nucleophiles used in this study.

The reaction of any one of **2a–g** with the nitrilium salt (Ph$_3$PCH$_2$Ph)[**1**] proceeds in MeCN or THF at RT over a period of 30 min giving 2-iminium *closo*-decaborates (Ph$_3$PCH$_2$Ph)[**3a–g**] in isolated yields of 59–92% (**Scheme 2**; for synthesis, characterization and discussion of spectral data see **Supporting Information**) as mixtures of the (*E*/*Z*)-isomers (for (Ph$_3$PCH$_2$Ph)[**3a–f**]), which varies for different products and ranges from 45/55 to 85/15. The benzophenone hydrazone derivative (Ph$_3$PCH$_2$Ph)[**3g**] exists exclusively in the (*Z*)-form, because of the availability of attractive non-covalent interactions B–H•••Ph (see later). The reaction of **2a** with (Ph$_3$PCH$_2$Ph)[**1**] proceeds in THF resulting in the formation of a precipitate of (Ph$_3$PCH$_2$Ph)[**3a**], whereas the reactions with **2b–g** do not result in spontaneous formation of precipitates.

NOS	R^1	*E*/*Z*-ratio	Yield (%)
(Ph$_3$PCH$_2$Ph)[**3a**]	H	45/55	92
(Ph$_3$PCH$_2$Ph)[**3b**]	Ac	85/15	75

NOS	R^2	R^3	*E*/*Z*-ratio	Yield (%)
(Ph$_3$PCH$_2$Ph)[**3c**]	NH$_2$	MeO	80/20	84
(Ph$_3$PCH$_2$Ph)[**3d**]	NH$_2$	H	75/25	58
(Ph$_3$PCH$_2$Ph)[**3e**]	NH$_2$	Br	70/30	59
(Ph$_3$PCH$_2$Ph)[**3f**]	NH$_2$	CF$_3$	70/30	68
(Ph$_3$PCH$_2$Ph)[**3g**]	Ph	H	0/100	78
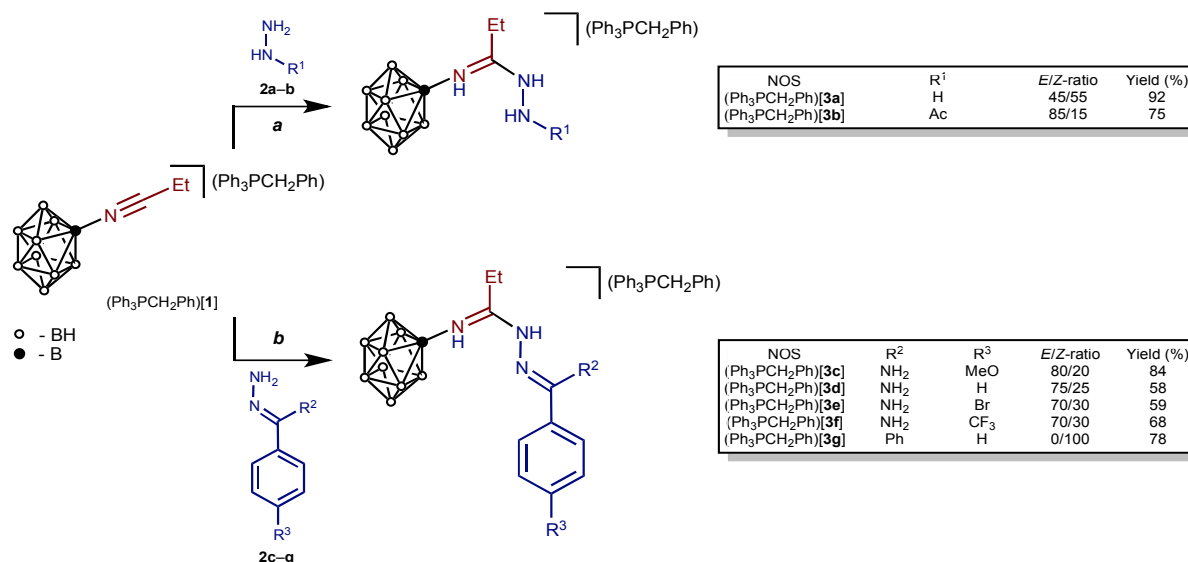
Scheme 2. Addition of the N(H)-nucleophiles to (Ph$_3$PCH$_2$Ph)[**1**].

Iminium salts (Ph$_3$PCH$_2$Ph)[**3a–g**] are stable at RT in air in the solid state for at least 3 months. In MeCN and toluene solutions, these compounds are stable for at least 1 week at RT and for 8 h at the boiling points of these solvents. These species decompose upon reflux in EtOH in the presence of NaOH (10 mol% respectively to (Ph$_3$PCH$_2$Ph)[**3a–g**], ca. 0.02 M solutions) giving (Ph$_3$PCH$_2$Ph)[B$_{10}$H$_9$NH$_3$], EtCO$_2^-$, and starting **2c–g**, which were detected by HRESI$^-$-MS (**2a** and **2b** are unobservable in the spectra due to *m/z* < 80 Da). Noticeably that in the cases of

(Ph₃PCH₂Ph)[**3b–f**] no formation of free or boron-bound 1,2,4-triazoles was detected by HRESI⁻-MS, in spite of the fact that these heterocycles are typically generated from acyl amidrazones.[18]

Theoretical Study of the Intramolecular Non-Covalent Interactions B–H•••π(Ph) in (Z)-(Ph₃PCH₂Ph)[3g]. Inspection of the crystallographic data reveals the presence of intramolecular non-covalent interactions B–H•••π(Ph) in crystal structure of (*Z*)-(Ph₃PCH₂Ph)[**3g**] (**Figure 1**). Indeed, the shortest distance H•••C in corresponding fragment of molecule is 2.99 Å, which is slightly larger than the sum of Bondi's (the shortest)[19] van der Waals radii of H and C atoms (2.90 Å), comparable with the sum of Alvarez's[20] van der Waals radii (2.97 Å), but lesser than sum of Rowland's[21] van der Waals radii (3.02 Å). Note that the van der Waals radius of the boron hydride hydrogen atom was supposed to be 1.39 Å as negatively charged thereby having increased atomic volume (instead of "classical" Bondi's van der Waals radius for H atom = 1.20 Å).[22] This type of non-covalent interactions is very rare and only few systems demonstrating such contacts were reported, viz. X-ray diffraction studies of [Cp*Ir(PR₃)S₂C₂B₁₀H₁₀] complexes reveal that the non-covalent interaction between the carborane B–H bonds and the phosphine aryl substituents involves a B–H•••π contacts (H•••π distances in these systems are 2.40−2.76 Å, which is significantly shorter than those in (*Z*)-(Ph₃PCH₂Ph)[**3g**]) (**Figure 1**).[23] Thus, in addition to the structural study, detailed computational analysis of the intramolecular non-covalent interactions B–H•••π(Ph) in crystal structure of (*Z*)-(Ph₃PCH₂Ph)[**3g**] is desirable.
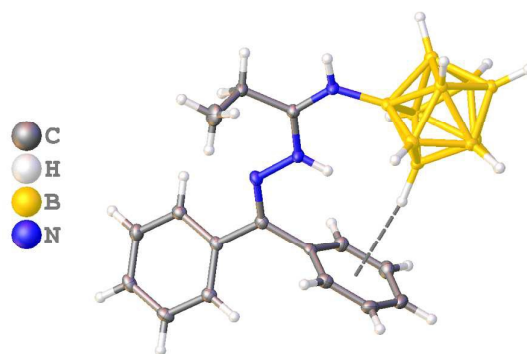
Figure 1. Molecular structure of (*Z*)-(Ph₃PCH₂Ph)[**3g**]. Thermal ellipsoids are given at the 50% probability level. Dotted line indicates the non-covalent intramolecular interactions B–H•••π(Ph).

In order to confirm or disprove the hypothesis on the existence of these non-covalent intramolecular interactions B–H•••π(Ph) in (Z)-(Ph$_3$PCH$_2$Ph)[**3g**] and to quantify their energy from a theoretical viewpoint, we carried out single point DFT calculations based on the experimental X-ray geometry of (Z)-(Ph$_3$PCH$_2$Ph)[**3g**] at the M06-2X/6-311++G** level of theory. We also performed topological analysis of the electron density distribution within the framework of Bader's theory (QTAIM method)[24] (**Table 1**). This approach has already been successfully used by us in studies of different non-covalent interactions and properties of coordination bonds in various transition metal complexes.[25] It is well-known that X-ray diffraction experiments cannot indicate the precise location of H atoms, and hydrogens are practically always placed at idealized positions even if a suitable electron density maximum could be found from a difference Fourier map. To obtain the theoretically (more correct) positions of H atoms and to exclude possible crystal packing effects, we have also carried out the geometry optimization procedure in the gas phase for (Z)-(Ph$_3$PCH$_2$Ph)[**3g**] and used the resulting equilibrium geometry for topological analysis of the electron density distribution. The contour line diagrams of the Laplacian distribution $\nabla^2\rho(\mathbf{r})$, bond paths, and selected zero-flux surfaces for non-covalent interactions B–H•••π(Ph) in (Z)-(Ph$_3$PCH$_2$Ph)[**3g**] are shown in **Figure 2**. To visualize the studied non-covalent interactions, reduced density gradient (RDG) analysis[26] was carried out, and RDG iso-surfaces for (Ph$_3$PCH$_2$Ph)[**3g**] were plotted (**Figure 2**).

Table 1. Values of the density of all electrons – $\rho(\mathbf{r})$, Laplacian of electron density – $\nabla^2\rho(\mathbf{r})$, energy density – H_b, potential energy density – $V(\mathbf{r})$, and Lagrangian kinetic energy – $G(\mathbf{r})$ (Hartree) at the bond critical points (3, –1), corresponding to non-covalent interactions B–H•••π(Ph) in(Z)-(Ph$_3$PCH$_2$Ph)[**3g**], bond lengths – l (Å), as well as energies of these interactions E_{int} (kcal mol^{-1}), defined by two approaches.*

DFT calculation based on the	$\rho(\mathbf{r})$	$\nabla^2\rho(\mathbf{r})$	H_b	$V(r)$	$G(r)$	E_{int} [a]	E_{int} [b]	l
Experimental X-ray geometry	0.006	0.016	0.000	−0.003	0.003	0.9	0.8	2.99
Equilibrium optimized	0.008	0.022	0.001	−0.004	0.005	1.3	1.4	2.93
geometry in gas phase	0.009	0.025	0.001	−0.004	0.005	1.3	1.4	2.80

[*] The Poincare–Hopf relationship is satisfied, thus all critical points have been found.

$$^a \; E_{int} = -V(\mathbf{r})/2 \; [27]$$

$$^b \; E_{int} = 0.429G(\mathbf{r}) \; [28]$$

Experimental X-ray geometry

Equilibrium optimized geometry in gas phase
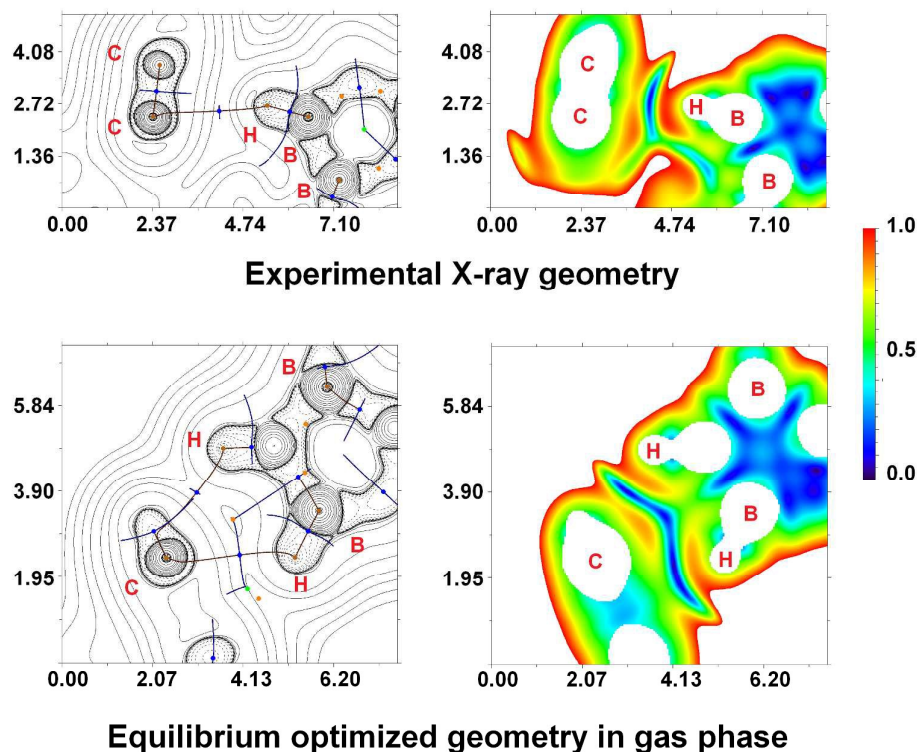
Figure 2. Contour line diagrams of the Laplacian distribution $\nabla^2\rho(\mathbf{r})$, bond paths and selected zero-flux surfaces (left) and RDG iso-surfaces (right) referring to the non-covalent interactions B–H•••π(Ph) in (*Z*)-(Ph₃PCH₂Ph)[**3g**] (M06-2X/6-311++G** level of theory). Bond critical points (3, –1) are shown in blue, nuclear critical points (3, –3) – in pale brown, ring critical points (3, +1) – in orange, and cage critical points (3, +3) – in light green. Length units – Å, RDG iso-surface values are given in Hartree.

The QTAIM analysis demonstrates the presence of appropriate bond critical points (BCPs) for non-covalent interactions B–H•••π(Ph) in (*Z*)-(Ph₃PCH₂Ph)[**3g**] both in solid state and in gas phase. The geometry optimization of (*Z*)-(Ph₃PCH₂Ph)[**3g**] led to shortening of B–H•••π(Ph) distances compared to the solid state geometry and to the formation of bifurcated contacts B–H•••C•••H–B. The low magnitude of the electron density (0.006–0.009 Hartree), positive values of the Laplacian (0.016–0.025 Hartree), and zero or close to zero (0.001 Hartree) positive energy density in these BCPs are typical for non-covalent interactions. We have defined energies for these contacts according to the procedures proposed by Espinosa et al.[27] and Vener et al.[28] (**Table 1**) and found that estimated strength of these non-covalent interactions is 0.8–1.4 kcal mol⁻¹. This is typical for weak hydrogen bonding following the classification of Jeffrey ("strong" H-bonds: 40–15 kcal mol⁻¹, "moderate" H-bonds: 15–4 kcal mol⁻¹, "weak" H-bonds: < 4 kcal mol⁻¹).[29] The balance between the Lagrangian kinetic energy $G(\mathbf{r})$ and potential energy density $V(\mathbf{r})$ at the BCPs reveals the nature of these interactions: if the ratio $-G(\mathbf{r})/V(\mathbf{r}) > 1$ is satisfied, then the nature of the appropriate interaction is purely non-covalent, while in case where $-G(\mathbf{r})/V(\mathbf{r}) < 1$ some covalent interaction also takes place.[30] Based on this criterion one can state that covalent contribution is absent in the B–H•••π(Ph) contacts in (*Z*)-(Ph₃PCH₂Ph)[**3g**], and as can be inferred from inspection of calculated NBO atomic charges, all C atoms in the Ph moiety involved in the non-covalent interactions B–H•••π(Ph) in (*Z*)-(Ph₃PCH₂Ph)[**3g**] are negatively charged (from –0.14 to –0.20), whereas the appropriate H centers are slightly positively (0.03) charged. However, it is of note that recently Hobza et al.[31] considered the nature of the non-covalent interactions in different B–H•••π(Ph) motifs and shown that it is not only electrostatically attractive non-classical hydrogen bonds, but rather non-specific weak dispersion-driven contacts.

The non-covalent interactions B–H•••π(Ph) determine the configuration of (*Z*)-(Ph₃PCH₂Ph)[**3g**]. Indeed, we performed geometry optimization procedure in the gas phase for other isomer of (*Z*)-(Ph₃PCH₂Ph)[**3g**] without non-covalent interactions B–H•••π(Ph) and found that this isomer is less stable (by 8.6 kcal mol⁻¹ in terms of Gibbs free energies) (**Table 4S**, **Supporting**

Information). It may thus be concluded that the contribution of these weak interactions to the stabilization of (*Z*)-(Ph$_3$PCH$_2$Ph)[**3g**] compared to isomerization is only 30–33%. The discussion about the theoretical calculations of relative energies for different isomers of this and other reported compounds in acetonitrile solution are given in the **Supporting Information (Tables 1S–3S)**.

Determination of Plausible Mechanism of Generation of (Ph$_3$PCH$_2$Ph)[3a–g].
(i) Kinetics. The kinetics of the nucleophilic addition of a range of nucleophiles (**2a–c** and **2e–g**; **Scheme 1**) to the nitrile moiety of the boron cluster was investigated next. Amidrazone **2d** gradually decomposed under the reaction conditions to give 3,6-diphenyl-1,2,4,5-tetrazine and no satisfactory kinetic data could thus be obtained for this species.[32] **Figure 3** shows a typical profile of the reaction progress as monitored by UV/Vis time-resolved spectrophotometry. The absorbance *vs*. time data was fitted to a single exponential as described previously,[33] yielding clean reactions.
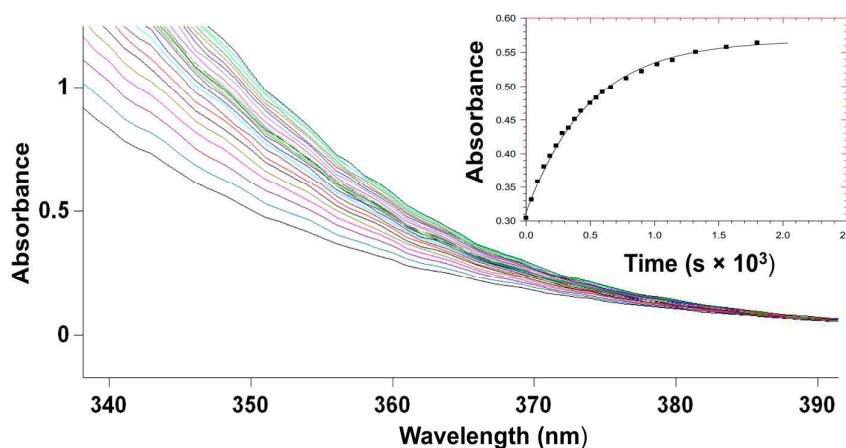
Figure 3. UV/Vis spectral changes of absorbance *vs*. time for the addition of nucleophile **2e** to (Ph$_3$PCH$_2$Ph)[**1**] (MeCN; 25 °C). Insert indicates fit of Abs.*vs* time data to a first-order exponential at 360 nm.[33] Δt = 0.75 min and 2 min, t$_{total}$ = 30 min. [**2e**] = 2.5×10^{-4} M, (Ph$_3$PCH$_2$Ph)[**1**] = 5×10^{-5} M.

To our surprise, a clear *second-order* [Nu(H)] dependence of the observed pseudo *first-order* rate constants was obtained, which at first glance might seem questionable considering the final

products (1:1 ratio of Nu(H) to the boron cluster) as isolated (see **Experimental Section** and **Figure 1**). However, as illustrated in **Figures 4, 5** and **7**, the experimental kinetic data clearly confirms the *second-order* dependence for all six the entering nucleophiles **2a–c** and **2e–g**. Visually this is manifested best by the logarithmic plots shown in **Figure 4**, which all yielded slopes equal to 2 within experimental error, see also **Table 2**.
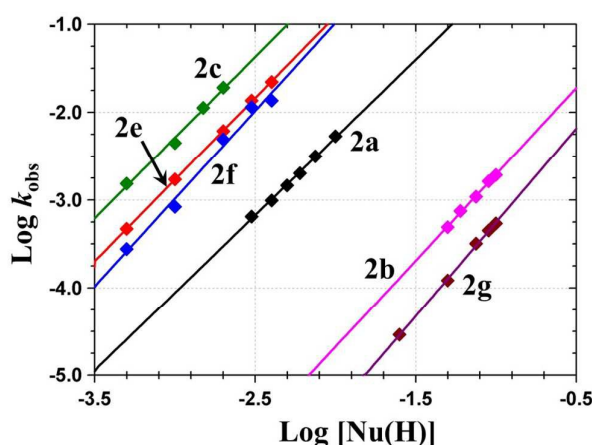
Figure 4. Plot of k_{obs} *vs.* entering log [Nu(H)] for the addition reaction of **2a–c** and **2e–g** to (Ph$_3$PCH$_2$Ph)[**1**] at 25 °C in MeCN, yielding linear plots with slopes *ca*. 2; (Ph$_3$PCH$_2$Ph)[**1**] = 5×10^{-5} M (λ = 330 nm).

Since similar behaviour has been reported in literature in distant related systems,[17d, e] we pursued the arguments further in more detail. Thus, where **Figure 4** clearly supports the *second-order* logarithmic dependence, **Figure 5** even more so, wherein the pseudo first-order kinetic data for all the entering nucleophiles were subjected to non-linear least-squares fits of the complete appropriate rate equation(s) as defined in **Scheme 3** (*a* and *b*) below, and clearly describe the exponential *second-order* increase in k_{obs} with increasing [**2**].
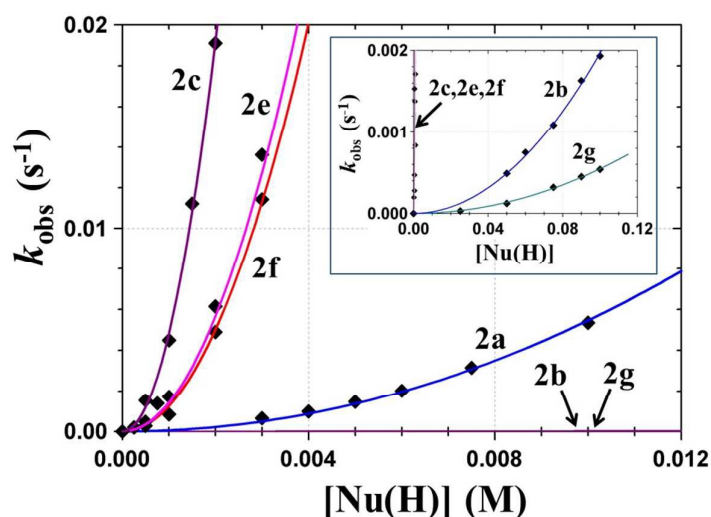
Figure 5. Plots of k_{obs} *vs.* [Nu(H)] for the nucleophilic addition of **2a–c** and **2e–g** to

(Ph$_3$PCH$_2$Ph)[**1**] at 25 °C in MeCN. Insert indicates slower nucleophiles (**2b** and **2g**; also both

exhibiting clear 2nd order behavior with respect to [Nu(H)]). Data are given in **Tables 5S** and **6S**.

(ii) Reaction Mechanism. We identified two likely scenarios for the kinetic behaviour and

the results obtained are therefore interpreted in cognisance of *second-order* [Nu(H)] behaviour as

presented in **Scheme 3** (*a* and *b*) below, respectively.

(a)

$$B + Nu(H) \underset{k_{-1}}{\overset{k_1,\, K_1}{\rightleftharpoons}} BNu(H) \qquad RDS \qquad (1a)$$

$$BNu(H) + Nu^*(H^*) \underset{k_{-2}}{\overset{k_2}{\rightleftharpoons}} \underset{\mathbf{3}}{BNu(H^*)} + Nu^*(H) \quad Fast \qquad (2a)$$
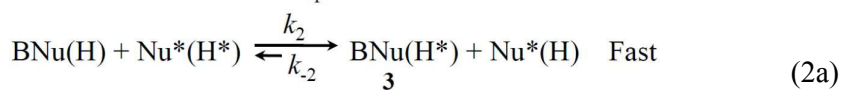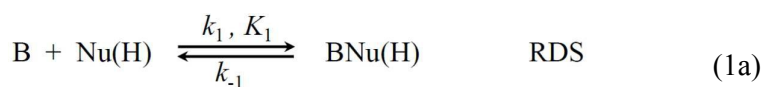
where RDS denotes the rate-determining step.

This yields the following Rate Law for the formation of **3** (with BNu(H) a steady state):

$$d[3]/dt = k_2[BNu(H)][Nu^*(H^*)] - k_{-2}[BNu(H^*)][Nu^*(H)] \quad (3a)$$

(b)

$$2\text{Nu(H)} \;\underset{k_{-1}}{\overset{k_1,\,K_1}{\rightleftharpoons}}\; [\text{Nu(H)}]_2 \qquad \text{Fast} \qquad (1b)$$

$$\text{B} + [\text{Nu(H)}]_2 \;\underset{k_{-2}}{\overset{k_2}{\rightleftharpoons}}\; \underset{\mathbf{2'}}{\text{B[Nu(H)]}_2} \qquad \text{RDS} \qquad (2b)$$

$$\text{B[Nu(H)]}_2 \;\rightleftharpoons\; \underset{\mathbf{3}}{\text{BNu(H)}} + \text{Nu(H)} \quad \text{Fast} \qquad (3b)$$
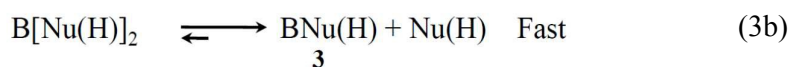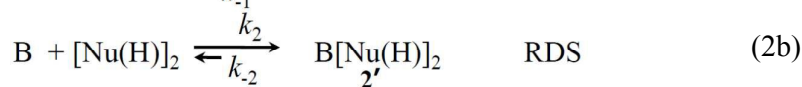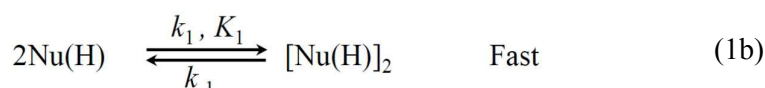
This yields the following Rate Law for the formation of **2′** (with $[\text{Nu(H)}]_2$ a steady state):

$$d[2']/dt = k_2 K_1 [\text{B}][\text{Nu(H)}]^2 - k_r [\text{B[Nu(H)]}_2] \qquad (4b)$$

Scheme 3. Reaction schemes for nucleophilic addition of **2a–c** and **2e–g** to $(\text{Ph}_3\text{PCH}_2\text{Ph})[\mathbf{1}]$, denoted by 'Nu(H)' and 'B', respectively. (a) Assuming a direct B–Nu attack (**Eq. 1a**) as a first rate-determining step followed by a fast proton exchange (**Eq. 2a**). To distinguish between the first Nu(H) involved in **Eq. 1a**, and the second nucleophile in **Eq. 2a**, asterisked nucleophiles are used. However, note that in all cases Nu(H) is identical to Nu*(H*). (b) Assuming a fast, bimolecular equilibrium-formation of a dinuclear $[\text{Nu(H)}]_2$ entity in **Eq. 1b**, which reacts in a rate-determining step with B (**Eq. 2b**), followed by a rapid loss of the extra Nu(H) to yield the final product BNu(H) (**3**) (**Eq. 3b**). In both **Scheme 3** (**a**) and (**b**) the reverse rate constant k_r is indicated but is not interpreted further.

As indicated in **Scheme 3**, two potential mechanisms were identified for the kinetics observed. The observed pseudo first-order rate constants for (**a**) and (**b**) are given by **Eq. 4a** and **Eq. 5b**, respectively, derived from basic kinetic principles and assuming $[\text{Nu(H)}] \gg [\text{B}]$.

Thus, firstly, as described in **Scheme 3** (**a**), a B–Nu(H) interaction (**Eq. 1a**) as a first rate-determining step is assumed, followed by a subsequent fast proton exchange (**Eq. 2a**). The pseudo *first-order* rate constant for this process is given by **Eq. 4a**. Motivation for this mechanism stems from analogous behavior of the oximes,[12a] as well as the assumed principle that the nucleophiles are expected to proceed via a direct attack at the boron cluster.

Under conditions where $[\text{Nu(H)}] \gg [\text{B}]$, the pseudo first-order rate constant is given by **Eq. 4a** after incorporating [BNu(H)] as a steady state:

$$k^{\mathrm{a}}_{\mathrm{obs}} = (k_1 K_{\mathrm{D}}[\mathrm{Nu(H)}]^2)/(1 + K_{\mathrm{D}}[\mathrm{Nu(H)}]) + k_{\mathrm{r}} \qquad (4a)$$

In **Eq. 4a**, $K_{\mathrm{D}} = k_2/k_{-1}$ = discrimination factor, *i.e.*, the ability of the boron cluster to discriminate between different entering nucleophiles, and k_{r} = reverse rate constant for the overall process.

Secondly, in **Scheme 3** (*b*) we consider a fast, bimolecular equilibrium-formation of a dinuclear $[\mathrm{Nu(H)}]_2$ entity in **Eq. 1b**, which reacts in a subsequent rate-determining step with B (**Eq. 2b**), followed by a rapid loss of the extra Nu(H) to yield the final product BNu(H) (**Eq. 3b**). The pseudo *first-order* rate constant for this process is given by **Eq. 5b**. Although one may envisage that the formal attack of $[\mathrm{Nu(H)}]_2$ should be potentially sterically inhibited in the dinuclear form, some evidence to its existence comes from the infrared spectra as presented in the **Supporting Information, Figure 54S**.

Under conditions where $[\mathrm{Nu(H)}] \gg [\mathrm{B}]$

$$d[\mathrm{B}]/[\mathrm{B}]d\mathrm{t} = k^{\mathrm{b}}_{\mathrm{obs}} = k_{\mathrm{f}}[\mathrm{Nu(H)}]^2 + k_{\mathrm{r}} \qquad (5b)$$

In **Eq. 5b**, $k_{\mathrm{f}} = k_2 K_1$ = forward *third-order* rate constant, and k_{r} = reverse rate constant for the overall process.

As illustrated in **Figures 4** and **5**, both rate laws as simplified in **Eqs. 4a** and **5b** describe the kinetics observed very well. In particular the logarithmic plots of both $k^{\mathrm{a}}_{\mathrm{obs}}$ and $k^{\mathrm{b}}_{\mathrm{obs}}$ *vs.* log[Nu(H)] in **Figure 4** which yield clear linear relationships with slopes close to 2 for all six nucleophiles **2a–c**, **2e–f**, see **Table 2**, convincingly support a 2nd order in [Nu(H)]. Similarly, **Figure 5** illustrates the plots of $k^{\mathrm{a}}_{\mathrm{obs}}$ and $k^{\mathrm{b}}_{\mathrm{obs}}$ *vs.* [Nu(H)] and the non-linear least-squares fits of the data to **Eqs. 4a** and **5b**, wherein good second-order fits for all six nucleophiles **2a–c**, **2e–f**, were obtained.

It is important to note that in the current study, the lack of solubility of the entering nucleophiles did not allow K_{D} to be separated from k_1 [i.e., in **Eq. 4a** $K_{\mathrm{D}}[\mathrm{Nu(H)}] \ll 1$], effectively yielding **Eq. 5b** shown above. An attempt to estimate a value for K_{D} is nevertheless illustrated in **Figure 56S** (see **Supporting Information**) by visually modelling the shape[34] and thus acceptable curves where values of K_{D} of 1–50 M^{-1} gave reasonable fits for nucleophile **2e**. However, for the

purpose of this study, and more importantly, to allow *direct* comparison between the two mechanisms as illustrated in **Scheme 3** (*a* and *b*) a $K_D = 1$ M^{-1} was utilised in all the fits involving **Eq. 4a.**

By performing experiments wherein the concentration of $(Ph_3PCH_2Ph)[\mathbf{1}]$ is in excess with respect to the entering nucleophile, we obtained the predicted *first-order* dependence on [B], see **Figure 6** (*a* and *b*). This was already illustrated in (and *required* from) both **Eq. 3a** and **4b**, which yields **Eq. 6ab** following least-squares analysis and incorporation of the second-order dependence of [Nu(H)]. Thus, under conditions where [B] >> [Nu(H)], both mechanisms in **Scheme 3** (*a* and *b*) and their rate laws in both **Eq. 3a** and **4b** simplifies to

$$d[Nu(H)]/[Nu(H)]dt = k^{ab}_{obs} = k_f{'}[B] + k_r \qquad (6ab)$$

where $k_f{'} = k_f X = k_1 K_D X$ (**Eq. 4a**) or $k_f = k_2 K_1 X$ (**Eq. 5b**), and $X = [Nu]$, to yield the corresponding third-order rate constants.
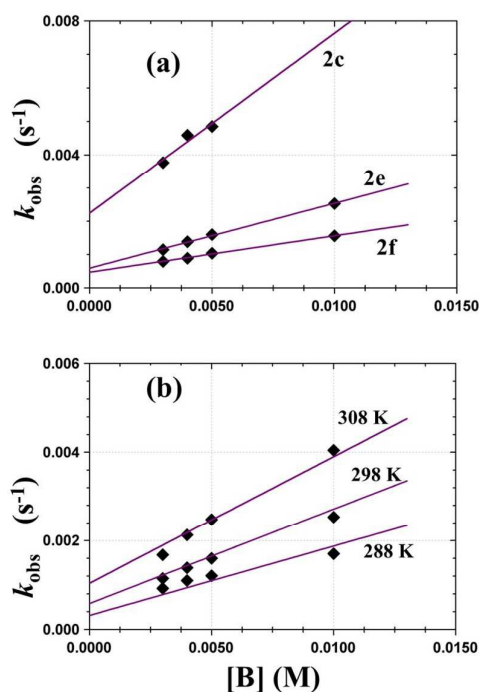
Figure 6. Plots of k_{obs} *vs*. [B] in MeCN for the nucleophilic addition of (a) **2c**, **2e** and **2f** to

(Ph$_3$PCH$_2$Ph)[**1**] at 25 °C; (b) **2e** to (Ph$_3$PCH$_2$Ph)[**1**] at different temperatures.

$$[Nu(H)] = 2.5 \times 10^{-4} \text{ M}.$$

In the case where [B] >> [Nu(H)], the pseudo *first-order* rate constants described by

Eq. 6ab yield reasonably similar forward *third-orde*r rate constants to those obtained when

monitoring the reactions with [Nu(H)] >> [B] (and utilising **Eqs. 4a** and **5b**), see **Table 2**,

considering the differences in experiments and solubility problems experience. This leads to the

conclusion that both reaction schemes [**Scheme 3** (*a* and *b*)] and the corresponding rate laws

appropriately describe the overall reaction. We take this as strong supporting evidence that we

selected appropriate reaction mechanisms in **Scheme 3**.

A clear non-zero small parallel/reverse reaction (intercept of linear dependence k^{ab}_{obs} *vs*. [B],

see **Figure 6** (*a* and *b*)) was obtained from this study. Although not as conclusive, the exponential

data wherein [Nu(H)] >> [B], as illustrated in **Figure 5**, could not *verify* this, but also not *exclude*

this since the standard deviations obtained do not allow accurate interpretation, see **Table 7S**. This

aspect is not considered further in this report since it does not really influence any conclusions

made.

We consider **Scheme 3** (*a*) the more likely mechanism since (*i*) the nucleophilic attack

seems the more likely reaction to be critically dependent on the electron density at the N atom and

(*ii*) intermolecular proton transfer and proton transfer reactions in general, are usually very fast.

For this latter process, **Eq. 4a** may be derived and clearly describes the kinetics observed,

yielding the appropriate rate constants as presented in **Tables 2** and **3**. This leaves us with a

mechanistic interpretation typical of many square-planar substitution reactions wherein a

'discriminating factor', *i.e*., the preference of the proton transfer (k_2) over the dissociation of the

entering nucleophile (k_{-1}) has been considered.[35] As indicated above, however, K_D ($=k_2/k_{-1}$) is

directly associated with k_1 and could not be separated therefrom ($k_f = k_1 K_D$) with all the data on

hand. Although one expects a variation in K_D, all relative trends therein are interpreted in combination with k_1, and therefore with respect to k_f.

   (iii) Variation of Entering Nucleophiles. The nucleophiles **2a–c** and **2e–g** as varied exhibited a significant range of almost *five* orders-of-magnitude in forward rate constants as manifested by k_f, with **2c** being the more reactive nucleophile and **2g** the least reactive (see **Figures 4** and **5**, and **Table 2**). Nucleophiles **2g** and **2b** appear to have low reactivity, with hydrazine intermediate, and the three electron-rich systems, **2e**, **2f** and, in particular, **2c** the most reactive.

Table 2. Rate constants for the nucleophilic addition of **2a–c** and **2e–g** to (Ph₃PCH₂Ph)[**1**] in MeCN at 25 °C; determined from least-squares fits of the observed pseudo *first-order* rate constants to **Eqs. 4a** and **5b**, and **Eq. 6ab,** which follows from (i.e., **Fig. 5**) as well as the logarithmic dependences as illustrated in **Fig. 4**

Nu(H)	Slopes from log plots [a]	k_f			k_r [d]
		Eq. **4a** (k_1K_D) [b] $(M^{-2}s^{-1})$	Eq. **5b** $(=k_2K_1)$ [c] $(M^{-2}s^{-1})$	Eq. **6ab** $(=k_2K_1)$ [d] $(M^{-2}s^{-1})$	(s^{-1})
2a	1.8±0.1	52±4	52±4	--	--
2b	1.8±0.1	0.21±0.04	0.19±0.02	--	--
2c	2.1±0.1	4794±81	4785±81	2200±300	0.0023± 0.0003
2e	2.0±0.2	1394±18	1388±18	800±80	0.0006±0.0001
2f	2.0±0.1	1285±35	1281±36	440±80	0.0005±0.0001
2g	1.9±0.1	0.06±0.03	0.06±0.02	--	--

   a) From slopes in **Fig. 4**. [b] Eq. 4a; Data in **Fig. 5**. [c] Eq. 5b; Data in **Fig. 5**. [d] Eq. 6ab; Data in **Fig. 6**

However, it must again be noted that the forward rate constants k_f as reported in **Tables 2–4** represent potential combinations of (*i*) rate (k_1) and discrimination constant (K_D) for the proposed mechanism in **Scheme 3** (*a*), [$k_f=k_1K_D$] or on the other hand (*ii*) rate k_2 and equilibrium constant for dinuclear [Nu(H)]₂ in the mechanism in **Scheme 3** (*b*) [$k_f=k_2K_1$]. Relative positions in the order are thus dependent on both these contributions and may not necessary be clearly defined. Nevertheless, it is noted that the forward rate constants k_f for the nucleophilic attack are in general agreement with

the nucleophiles' expected coordinating and accepted electron donating capabilities, and indeed, spanning a *significan*t five orders-of-magnitude range of *reactivities*.

(iv) Activation parameters. **Figure 7** illustrates the temperature dependence of the observed pseudo first-order rate constants for the nucleophilic addition of **2e** to (Ph$_3$PCH$_2$Ph)[**1**]. The lines represent the least-squares fitted values for the experimental data points to a global model of the exponential form of the Eyring equation, as reported previously.[35] This yields a very low $\Delta H^{\neq} = (6.9 \pm 0.8)$ kJ·mol^{-1} and large negative $\Delta S^{\neq} = (-195 \pm 3)$ J·K^{-1}·mol^{-1}, see **Table 3**.

Values for the activation parameters for **2c** and **2f** as entering nucleophiles were also obtained and are given in **Table 3** (for experimental fits, see **Supporting information; Table 8S**).
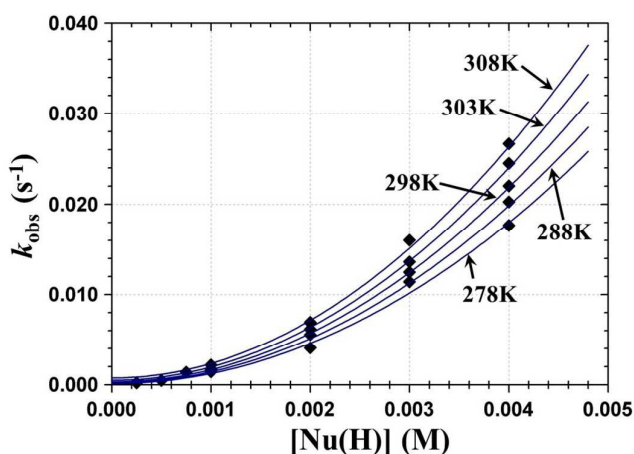
Figure 7. Global fit of the observed pseudo *first-order* rate constants (at different temperatures) to the exponential form of the Eyring equation for the addition of **2e** to (Ph$_3$PCH$_2$Ph)[**1**] in MeCN.

Table 3. Data from least-squares fit of the observed pseudo first-order rate constants for the nucleophilic addition of **2c**, **2e**, and **2f** to (Ph$_3$PCH$_2$Ph)[**1**] in MeCN.

Constant	Temp (°C)	2c **Fig. 6S** Eq. Eq. 4a [a]	2e **Fig. 5** Eq. 4a [a]	2e **Fig. 5** Eq. 5b [b]	2f **Fig. 6S** Eq. 4a [a]
k_f (M^{-2} s^{-1})	35	--	1698±29	1654±52	1037±28
	30	--	1543±33	1512±53	--
	25	4785±81	1417±29	1388±18	865±33
	15	--	1300±29	1255±52	621±33
	5	--	1138±29	1119±52	--

$\Delta H^{\neq}$ (kJ mol^{-1})	--	14±2 [a)]	6.9±0.8 [a)]	6.1±0.7 [b)]	15±1 [a)]
$\Delta S^{\neq}$ (J K^{-1} mol^{-1})	--	−162±6 [a)]	−195±3 [a)]	−164±3 [b)]	−139±4 [a)]

[a)] Data from global fits of k_{obs} *vs.* [**2c**], [**2e**] and [**2f**] to **Eq. 4a** at different temperatures. [b)] Data from global fits of k_{obs} *vs.* [**2e**] to **Eq. 5b** at different temperatures.

The activation parameters for the nucleophilic addition of **2e** to (Ph$_3$PCH$_2$Ph)[**1**] yield as indicated the very low $\Delta H^{\neq}$ = (6.9±0.6) kJ mol^{-1} and large negative $\Delta S^{\neq}$ = (−195±3) J K^{-1} mol^{-1}, and indicate that the reaction is primarily entropy controlled, with $\Delta S^{\neq}$ contributing 87% to the Gibbs free energy of activation at 25 °C, see **Table 4**. The values for the activation parameters for **2c** and **2f** as entering nucleophiles are comparable to that of **2e**, with $\Delta S^{\neq}$ contributing some 73% of the Gibbs free energy of activation at 25 °C in both. This is in general agreement with the literature values on related reactions,[33] and indicate smaller contributions of bond formation to the total Gibbs' energy of activation in these systems.

Table 4. Data from least-squares fits of the observed pseudo first-order rate constants [via a global fit[33]] for the nucleophilic addition of **2c**, **2e** and **2f** to (Ph$_3$PCH$_2$Ph)[**1**] in MeCN at 25°C.

Nucleophile	2c	2e	2f
k_f (M^{-2} s^{-1})	4785±81	1388±18	865±33
$\Delta H^{\neq}$ (kJ mol^{-1})	14±2 [a,b)]	6.9±0.8 [b)]	15±1 [b)]
$\Delta S^{\neq}$ (J K^{-1} mol^{-1})	−162±6 [a,b)]	−195±3 [b)]	−139±4 [b)]
$\Delta G^{\neq\,298}$ (kJ mol^{-1})	52±4	65±1	56±2
$\Delta S^{\neq}$ fraction of $\Delta G^{\neq}$ (%)	73	89	73

[a)]$\Delta H^{\neq}$ = 21±3 kJ·mol^{-1}, $\Delta S^{\neq}$ = (-121±11 J·K^{-1}·mol^{-1}) from **Fig. 5(b)**; [b)] Data from individual fits of k_{obs} *vs.* [**2e**] to **Eq. 3** at different temperatures; see Table 3.

Conclusions

The nucleophilic addition to the C≡N group of the 2-propanenitrilium *closo*-decaborate cluster of three types of N(H)-nucleophiles, viz. hydrazine, acetyl hydrazide, and a set of hydrazones giving *N-closo*-decaborato amidrazones has been studied. In the X-ray structure of (*Z*)-(Ph$_3$PCH$_2$Ph)[**3g**], very rare intramolecular non-covalent interactions B–H•••π(Ph) were detected and studied by DFT calculations (M06-2X/6-311++G** level of theory) and topological analysis of the electron density distribution within the framework of Bader's theory (QTAIM method).

New Journal of Chemistry Accepted Manuscript

Estimated strength of these non-covalent interactions is 0.8–1.4 kcal/mol. A systematic mechanistic study of the nucleophilic addition was undertaken and included detailed synthetic, crystallographic, computational and kinetic work. As a result, a nucleophilicity series for the N(H)-nucleophiles, with a range of structural types, was obtained. A clear *second*-order dependence on the entering nucleophiles has been obtained for all six the nucleophiles, yielding overall *third-order* kinetics and the reactivities ranged over *five* orders-of-magnitude.

Based upon the experimental data, two possible mechanisms have been proposed. The first possibility includes a consecutive incorporation of two Nu(H) nucleophiles, with the second step responsible for a subsequent rapid proton exchange. The second possible mechanism assumes a pre-formation of a dinuclear $[Nu(H)]_2$ species, which subsequently proceeds with the nucleophilic attack on the boron cluster. We consider that the first mechanism is more plausible since (*i*) the nucleophilic attack seems the more likely reaction to be critically dependent on the electron density at the N atom and (*ii*) intermolecular proton transfer, and proton transfer reactions in general, are usually very fast. The activation parameters for amidrazones employed as N(H)-nucleophiles indicate a small dependence on bond formation, but significantly negative entropies of activation with the latter contributing ca. 70–80% of the total Gibbs free energy of activation, $\Delta G^{\neq}$.

Thus, this work provides a broad series of nucleophilicity of Nu(H)-nucleophiles with wide-ranging variation of their structural types (**Scheme 1**). Although the obtained series follow general principles of physical organic chemistry, the quantitative data are certainly helpful for planning physical chemistry experiments. Moreover, metal-free and metal-involving nucleophilic additions of N(H)-nucleophiles comprise a field of intensive studies, and we believe that our nucleophilicity series will be useful to control various nucleophilic additions of N-donors. Further development of kinetics and reaction mechanisms of addition of other nucleophiles to 2-nitrilium *closo*-decaborates is underway in our group.

Experimental Section

Materials and Instrumentation. Solvents MeCN, Et$_2$O, CH$_2$Cl$_2$, ^{i}PrOH and 1 M hydrazine solutions in MeCN and in THF were obtained from commercial sources and used as received. Benzyltriphenylphosphonium 2-nitrilium-*closo*-decaborate, (Ph$_3$PCH$_2$Ph)[**1**],[36] acetyl hydrazide **2b**,[37] and benzophenone hydrazone **2g**[38] were synthesized according to the literature methods. Melting points were measured on a Stuart SMP30 apparatus in capillaries and are not corrected. Elemental analysis for boron was performed by the FSUE IREA 291 Center (Moscow) on an aiCAP 6300 Duo ICP spectrometer using H$_3$BO$_3$ as an internal standard. Electrospray ionization mass spectra were obtained on a Bruker micrOTOF spectrometer equipped with an electrospray ionization (ESI) source. The instrument was operated both in negative and in positive ion modes using an m/z range of 50–3000. The nebulizer gas flow was 0.4 bar, and the drying gas flow was 4.0 L/min. For ESI, the clusters were dissolved in MeOH. In the isotopic pattern, the most intensive peak is reported. Molar conductivities of $7{\times}10^{-4}$ M solutions in MeCN were measured on a Mettler Toledo FE30 conductometer using an Inlab710 sensor. Infrared spectra (3600–500 cm^{-1}) were recorded on a Shimadzu IR Prestige-21 instrument in KBr pellets. ^{1}H{^{11}B} and ^{11}B{^{1}H} NMR spectra were measured on a Bruker Avance 400 spectrometer in CD$_3$CN at ambient temperature; residual solvent signals were used as the internal standard for ^{1}H{^{11}B} and ^{13}C{^{1}H} NMR, whereas BF$_3$•Et$_2$O was used as the external standard for ^{11}B{^{1}H} NMR.

X-ray Structure Determination. A single-crystal X-ray diffraction experiment was carried out using Agilent Technologies «Xcalibur» ((*Z*)-(Ph$_3$PCH$_2$Ph)[**3b**]•MeCN, (Ph$_3$PCH$_2$Ph)[**3d**]•MeCN, and (*Z*)-(Ph$_3$PCH$_2$Ph)[**3g**]•MeCN) and «SuperNova» ((*E*)-(Ph$_3$PCH$_2$Ph)[**3a**]•MeCN, (*Z*)-(Ph$_3$PCH$_2$Ph)[**3c**], (*E*)-(Ph$_3$PCH$_2$Ph)[**3e**], and (*E*)-(Ph$_3$PCH$_2$Ph)[**3f**]) diffractometers with monochromated MoKα or CuKα radiation, respectively. The studied crystals were kept at 100(2) K during data collection. The structures had been solved by the Superflip[39] structure solution program using Charge Flipping and refined by means of the ShelXL[40] program, incorporated in the OLEX2 program package.[41] Empirical absorption correction was applied in CrysAlisPro[42] program complex using spherical harmonics, implemented in SCALE3 ABSPACK

scaling algorithm. CCDC numbers 1563793–1563799 contains the supplementary crystallographic data for this paper. These data can be obtained free of charge from the Cambridge Crystallographic Data Centre viawww.ccdc.cam.ac.uk/data_request/cif.

Kinetic Equipment and Procedures. Exploratory UV/visible measurements were performed on a Varian Cary 50 Conc UV–visible spectrophotometer with thermostated automated multicell changers (10 cells virtually simultaneously monitored) equipped with a JulaboF12-mV temperature cell regulator (accurate within 0.1 °C) in 1.000±0.001 cm quartz tandem cuvette cells. **Figure 3** shows a typical time-resolved reaction progress monitored by UV/vis. Reactions were also monitored by ^{1}H NMR where appropriate and the rates and products obtained where in agreement with the UV/vis measurements.

Kinetic Data Treatment. Stability tests were conducted over several days on a UV–vis spectrometer for (Ph$_3$PCH$_2$Ph)[**1**] and nucleophiles **2a–c**; **2e–g** to ensure no decomposition occurred. However, amidrazone **2d** gradually decomposed to give 3,6-diphenyl-1,2,4,5-tetrazine.[32] Because of the good solubility of (Ph$_3$PCH$_2$Ph)[**1**] only in CH$_2$Cl$_2$ and MeCN among most common organic solvents, all the reactions were performed in MeCN, which is a more convenient solvent for variable temperature experiments.

Computational Details. The full geometry optimization and single point calculations based on the experimental X-ray geometries have been carried out at the DFT level of theory using the M06-2X functional (this functional parameterized for main-group elements and specifically developed to describe weak dispersion forces and non-covalent interactions)[43] with the help of Gaussian-09 program package.[44] The standard 6-311++G** basis sets were used for all atoms. No symmetry restrictions have been applied during the geometry optimization. The Hessian matrix was calculated analytically for optimized structures in order to prove the location of correct minima (no imaginary frequencies), and to estimate the thermodynamic parameters, the latter being calculated at 25 °C. The solvent effects were taken into account using the SMD continuum solvation model by Truhlar and coworkers[45] with acetonitrile as solvent. The topological analysis of the electron

density distribution with the help of the atoms in molecules (QTAIM) method developed by Bader[24] has been performed by using the Multiwfn program (version 3.3.7).[46] The atomic charges were computed by using the natural bond orbital (NBO) partitioning scheme.[47] The Cartesian atomic coordinates for all model species are presented in **Table 4S** (**Supporting Information**).

ASSOCIATED CONTENT

The Supporting Information is available free of charge on the…

AUTHOR INFORMATION

Corresponding Authors

*E-mail: d.s.bolotin@spbu.ru (D.S.B.)

*E-mail: roodta@ufs.ac.za (A.R.)

Notes

The authors declare no competing financial interest.

ACKNOWLEDGMENTS

Center for Chemical Analysis and Materials Research (all belong to Saint Petersburg State University).

REFERENCES

1. (a) A. D. Yapryntsev, A. Y. Bykov, A. E. Baranchikov, K. Y. Zhizhin, V. K. Ivanov and N. T. Kuznetsov, *Inorg. Chem.*, 2017, **56**, 3421–3428; (b) R. Cheng, Z. Qiu and Z. Xie, *Nat. Commun.*, 2017, **8**, 14827; (c) R. M. Dziedzic, J. L. Martin, J. C. Axtell, L. M. A. Saleh, T. C. Ong, Y. F. Yang, M. S. Messina, A. L. Rheingold, K. N. Houk and A. M. Spokoyny, *J. Am. Chem. Soc.*, 2017, **139**, 7729–7732; (d) J. Estrada and V. Lavallo, *Angew. Chem. Int. Ed.*, 2017, **56**, 1–5; (e) A. I. Wixtrom, Y. Shao, D. Jung, C. W. Machan, S. N. Kevork, E. A. Qian, J. C. Axtell, S. I. Khan, C. P. Kubiak and A. M. Spokoyny, *Inorg. Chem. Front.*, 2016, **3**, 711–717; (f) M. S. Messina, J. C. Axtell, Y. Wang, P. Chong, A. I. Wixtrom, K. O. Kirlikovali, B. M. Upton, B. M. Hunter, O. S. Shafaat, S. I. Khan, J. R. Winkler, H. B. Gray, A. N. Alexandrova, H. D. Maynard and A. M. Spokoyny, *J. Am. Chem. Soc.*, 2016, **138**, 6952–6955; (g) R. M. Dziedzic, L. M. Saleh, J. C. Axtell, J. L. Martin, S. L. Stevens, A. T. Royappa, A. L. Rheingold and A. M. Spokoyny, *J. Am. Chem. Soc.*, 2016, **138**, 9081–9084; (h) Y. O. Wong, M. D. Smith and D. V. Peryshkov, *Chem.–Eur. J*, 2016, **22**, 6764–6767.

2. (a) T. Wütz, F. Diab and L. Wesemann, *Eur. J. Inorg. Chem.*, 2017, **38–39**, 4645–4652; (b) J. Estrada, C. A. Lugo, S. G. McArthur and V. Lavallo, *Chem. Commun.*, 2016, **52**, 1824–1826; (c) B. J. Eleazer, M. D. Smith and D. V. Peryshkov, *Organometallics*, 2016, **35**, 106–112; (d) R. D. Adams, J. Kiprotich, D. V. Peryshkov and Y. O. Wong, *Chem.–Eur. J*, 2016, **22**, 6501–6504; (e) K. O. Kirlikovali, J. C. Axtell, A. Gonzalez, A. C. Phung, S. I. Khan and A. M. Spokoyny, *Chem. Sci.*, 2016, **7**, 5132–5138; (f) J. C. Axtell, K. O. Kirlikovali, P. I. Djurovich, D. Jung, V. T. Nguyen, B. Munekiyo, A. T. Royappa, A. L. Rheingold and A. M. Spokoyny, *J. Am. Chem. Soc.*, 2016, **138**, 15758–15765.

3. (a) M. F. Hawthorne and A. Maderna, *Chem. Rev.*, 1999, **99**, 3421–3434; (b) M. Couto, I. Mastandrea, M. Cabrera, P. Cabral, F. Teixidor, H. Cerecetto and C. Vinas, *Chem.–Eur. J.*, 2017, **23**, 9233–9238; (c) P. Mi, H. Yanagie, N. Dewi, H. C. Yen, X. Liu, M. Suzuki, Y. Sakurai, K. Ono, H. Takahashi, H. Cabral, K. Kataoka and N. Nishiyama, *J. Control. Release*, 2017, **254**, 1–9; (d) P. J. Kueffer, C. A. Maitz, A. A. Khan, S. A. Schuster, N. I. Shlyakhtina, S. S. Jalisatgi, J. D. Brockman, D. W. Nigg and M. F. Hawthorne, *Proc. Natl. Acad. Sci. U. S. A.*, 2013, **110**, 6512–6517; (e) D. A. Feakes, *Boron Sci.*, 2012, 277–291; (f) G. Calabrese, J. J. Nesnas, E. Barbu, D. Fatouros and J. Tsibouklis, *Drug Discov. Today*, 2012, **17**, 153–159; (g) Z. J. Lesnikowski, *Boron Sci.*, 2012, 3–19.

4. P. Cigler, M. Kozisek, P. Rezacova, J. Brynda, Z. Otwinowski, J. Pokorna, J. Plesek, B. Gruner, L. Doleckova-Maresova, M. Masa, J. Sedlacek, J. Bodem, H. G. Krausslich, V. Kral and J. Konvalinka, *Proc. Natl. Acad. Sci. U. S. A.*, 2005, **102**, 15394–15399.

5. (a) W. C. Ewing, P. J. Carroll and L. G. Sneddon, *Inorg. Chem.*, 2008, **47**, 8580–8582; (b) D. Naoufal, M. Kodeih, D. Cornu and P. Miele, *J. Organomet. Chem.*, 2005, **690**, 2787–2789.

6. R. A. Watson-Clark and M. F. Hawthorne, *Inorg. Chem.*, 1997, **36**, 5419–5420.

7. D. S. Wilbur, M.-K. Chyan, D. K. Hamlin, R. L. Vessella, T. J. Wedge and M. F. Hawthorne, *Bioconjugate Chem.*, 2007, **18**, 1226–1240.

8. (a) I. N. Klyukin, A. P. Zhdanov, E. Y. Matveev, G. A. Razgonyaeva, M. S. Grigoriev, K. Y. Zhizhin and N. T. Kuznetsov, *Inorg. Chem. Commun.*, 2014, **50**, 28–30; (b) A. S. Kubasov, E. Y. Matveev, V. M. Retivov, S. S. Akimov, G. A. Razgonyaeva, I. N. Polyakova, N. A. Votinova, K. Y. Zhizhin and N. T. Kuznetsov, *Russ. Chem. Bull.*, 2014, **63**, 187–193; (c) E. F. Safronova, V. V. Avdeeva, I. N. Polyakova, A. V. Vologzhanina, L. V. Goeva, E. A. Malinina and N. T. Kuznetsov, *Dokl. Chem.*, 2013, **452**, 240–244; (d) V. I. Bragin, I. B. Sivaev, V. I. Bregadze and N. A. Votinova, *J. Organomet. Chem.*, 2005, **690**, 2847–2849.

9. I. B. Sivaev, N. A. Votinova, V. I. Bragin, Z. A. Starikova, L. V. Goeva, V. I. Bregadze and S. Sjoberg, *J. Organomet. Chem.*, 2002, **657**, 163–170.

10.   A. L. Mindich, N. A. Bokach, M. L. Kuznetsov, M. Haukka, A. P. Zhdanov, K. Y. Zhizhin, S. A. Miltsov, N. T. Kuznetsov and V. Y. Kukushkin, *ChemPlusChem*, 2012, **77**, 1075–1086.

11.   (a) K. A. Zhdanova, A. P. Zhdanov, A. V. Ezhov, N. A. Bragina, K. Y. Zhizhin, I. P. Ushakova, A. F. Mironov and N. T. Kuznetsov, *Russ. Chem. Bull.*, 2014, **63**, 194–200; (b) A. P. Zhdanov, I. N. Polyakova, G. A. Razgonyaeva, K. Y. Zhizhin and N. T. Kuznetsov, *Russ. J. Inorg. Chem.*, 2011, **56**, 847–855.

12.   (a) D. S. Bolotin, V. K. Burianova, A. S. Novikov, M. Y. Demakova, C. Pretorius, P. P. Mokolokolo, A. Roodt, N. A. Bokach, V. V. Suslonov, A. P. Zhdanov, K. Y. Zhizhin, N. T. Kuznetsov and V. Y. Kukushkin, *Organometallics*, 2016, **35**, 3612–3623; (b) A. P. Zhdanov, M. V. Lisovsky, L. V. Goeva, G. A. Razgonyaeva, I. N. Polyakova, K. Y. Zhizhin and N. T. Kuznetsov, *Russ. Chem. Bull.*, 2009, **58**, 1694–1700.

13.   A. L. Mindich, N. A. Bokach, F. M. Dolgushin, M. Haukka, L. A. Lisitsyn, A. P. Zhdanov, K. Y. Zhizhin, S. A. Miltsov, N. T. Kuznetsov and V. Y. Kukushkin, *Organometallics*, 2012, **31**, 1716–1724.

14.   A. L. Mindich, N. A. Bokach, M. L. Kuznetsov, G. L. Starova, A. P. Zhdanov, K. Y. Zhizhin, S. A. Miltsov, N. T. Kuznetsov and V. Y. Kukushkin, *Organometallics*, 2013, **32**, 6576–6586.

15.   G. Froehner, K. Challis, K. Gagnon, T. Getman and R. Luck, *Synth. React. Inorg. Met.-Org. Nano-Met. Chem.*, 2006, **36**, 777–785.

16.   V. Sicha, J. Plesek, M. Kvicalova, I. Cisarova and B. Gruner, *Dalton Trans.*, 2009, DOI: 10.1039/b814941k, 851–860.

17.   (a) N. C. de Lucas, J. C. Netto-Ferreira, J. Andraos and J. C. Scaiano, *J. Org. Chem.*, 2001, **66**, 5016–5021; (b) C. Brinkmann, A. G. Barrett, M. S. Hill and P. A. Procopiou, *J. Am. Chem. Soc.*, 2012, **134**, 2193–2207; (c) H. K. Oh and J. M. Lee, *Bull. Korean Chem. Soc.*, 2002, **23**, 1459–1462; (d) L. Calligaro, P. Uguagliati, B. Crociani and U. Belluco, *J. Organomet. Chem.*, 1975, **92**, 399–408; (e) R. J. Angelici and R. W. Brink, *Inorg. Chem.*, 1973, **12**, 1067–1071.

18.   (a) J. Sanning, L. Stegemann, P. R. Ewen, C. Schwermann, C. G. Daniliuc, D. Zhang, N. Lin, L. Duan, D. Wegner, N. L. Doltsinis and C. A. Strassert, *J. Mater. Chem. C*, 2016, **4**, 2560–2565; (b) M. Mydlak, C. H. Yang, F. Polo, A. Galstyan, C. G. Daniliuc, M. Felicetti, J. Leonhardt, C. A. Strassert and L. De Cola, *Chem.–Eur. J*, 2015, **21**, 5161–5172; (c) B. Barlaam, S. Cosulich, B. Delouvrie, R. Ellston, M. Fitzek, H. Germain, S. Green, U. Hancox, C. S. Harris, K. Hudson, C. Lambert-van der Brempt, H. Lebraud, F. Magnien, M. Lamorlette, A. Le Griffon, R. Morgentin, G. Ouvry, K. Page, G. Pasquet, U. Polanska, L. Ruston, T. Saleh, M. Vautier and L. Ward, *Bioorg. Med. Chem. Lett.*, 2015, **25**, 5155–5162.

19.   (a) A. Bondi, *J. Phys. Chem.*, 1966, **70**, 3006–3007; (b) A. Bondi, *J. Phys. Chem.*, 1964, **68**, 441–451.

20.   S. Alvarez, *Dalton Trans.*, 2013, **42**, 8617–8636.

21.   R. S. Rowland and R. Taylor, *J. Phys. Chem.*, 1996, **100**, 7384–7391.

22.   D. J. Wolstenholme, J. Flogeras, F. N. Che, A. Decken and G. S. McGrady, *J. Am. Chem. Soc.*, 2013, **135**, 2439–2442.

23.   (a) X. Zhang, H. Dai, H. Yan, W. Zou and D. Cremer, *J. Am. Chem. Soc.*, 2016, **138**, 4334–4337; (b) W. Zou, X. Zhang, H. Dai, H. Yan, D. Cremer and E. Kraka, *J. Organomet. Chem.*, 2018, DOI: 10.1016/j.jorganchem.2018.1002.1014.

24.   R. F. W. Bader, *Atoms in Molecules: A Quantum Theory*, Oxford University Press, Oxford, 1990.

25.   (a) K. I. Kulish, A. S. Novikov, P. M. Tolstoy, D. S. Bolotin, N. A. Bokach, A. A. Zolotorev and V. Y. Kukushkin, *J. Mol. Struct.*, 2016, **1111**, 142–150; (b) D. M. Ivanov, Y. V. Kirina, A. S. Novikov, G. L. Starova and V. Y. Kukushkin, *J. Mol. Struct.*, 2016, **1104**, 19–23; (c) D. M. Ivanov, A. S. Novikov, G. L. Starova, M. Haukka and V. Y. Kukushkin, *CrystEngComm*, 2016, **18**, 5278–5286; (d) T. V. Serebryanskaya, A. S. Novikov, P. V.

Gushchin, M. Haukka, R. E. Asfin, P. M. Tolstoy and V. Y. Kukushkin, *Phys. Chem. Chem. Phys.*, 2016, **18**, 14104–14112; (e) A. A. Melekhova, A. S. Novikov, K. V. Luzyanin, N. A. Bokach, G. L. Starova, V. V. Gurzhiy and V. Y. Kukushkin, *Inorg. Chim. Acta*, 2015, **434**, 31–36.

26. E. R. Johnson, S. Keinan, P. Mori-Sanchez, J. Contreras-Garcia, A. J. Cohen and W. Yang, *J. Am. Chem. Soc.*, 2010, **132**, 6498–6506.

27. E. Espinosa, E. Molins and C. Lecomte, *Chem. Phys. Lett.*, 1998, **285**, 170–173.

28. M. V. Vener, A. N. Egorova, A. V. Churakov and V. G. Tsirelson, *J. Comput. Chem.*, 2012, **33**, 2303–2309.

29. G. A. Jeffrey, *An Introduction to Hydrogen Bonding*, Oxford University Press, Oxford, 1997.

30. E. Espinosa, I. Alkorta, J. Elguero and E. Molins, *J. Chem. Phys.*, 2002, **117**, 5529–5542.

31. J. Fanfrlik, A. Pecina, J. Rezac, R. Sedlak, D. Hnyk, M. Lepsik and P. Hobza, *Phys. Chem. Chem. Phys.*, 2017, **19**, 18194–18200.

32. R. N. Warrener, in *e-EROS Encyclopedia of Reagents for Organic Synthesis*, John Wiley & Sons, Ltd, Chichester, UK, 2003.

33. (a) M. Schutte, G. Kemp, H. G. Visser and A. Roodt, *Inorg. Chem.*, 2011, **50**, 12486–12498; (b) M. Schutte, A. Roodt and H. G. Visser, *Inorg. Chem.*, 2012, **51**, 11996–12006; (c) A. Brink, H. G. Visser and A. Roodt, *Inorg. Chem.*, 2013, **52**, 8950–8961; (d) C. Hennion, K. J. Jonasson, O. F. Wendt and A. Roodt, *Dalton Trans.*, 2013, **42**, 14134–14139; (e) A. Brink, I. Truedsson, A. Fleckhaus, M. T. Johnson, P. O. Norrby, A. Roodt and O. F. Wendt, *Dalton Trans.*, 2014, **43**, 8894–8898; (f) A. Brink, H. G. Visser and A. Roodt, *Inorg. Chem.*, 2014, **53**, 12480–12488; (g) A. Frei, D. Sidler, P. Mokolokolo, H. Braband, T. Fox, B. Spingler, A. Roodt and R. Alberto, *Inorg. Chem.*, 2016, **55**, 9352–9360.

34. (a) A. Roodt, J. G. Leipoldt, L. Helm and A. E. Merbach, *Inorg. Chem.*, 1994, **33**, 140–147; (b) A. Roodt, H. G. Visser and A. Brink, *Crystallogr. Rev.*, 2011, **17**, 241–280; cA. Roodt, A. Abou-Hamdan, H. P. Engelbrecht and A. E. Merbach, *Adv. Inorg. Chem.*, 2000, **49**, 59–126.

35. (a) R. G. Wilkins, *Kinetics and Mechanism of Reactions of Transition Metal Complexes*, Wiley-VCH Verlag, 2nd edn., 2003; (b) R. Romeo, G. Arena, L. Monsu Scolaro and M. R. Plutino, *Inorg. Chim. Acta*, 1995, **240**, 81–92; (c) R. Romeo, A. Grassi and L. Monsu Scolaro, *Inorg. Chem.*, 1992, **31**, 4383–4390.

36. D. Dou, I. J. Mavunkal, J. A. Krause Bauer, C. B. Knobler, M. F. Hawthorne and S. G. Shore, *Inorg. Chem.*, 1994, **33**, 6432–6434.

37. B. Sadek, J. S. Schwed, D. Subramanian, L. Weizel, M. Walter, A. Adem and H. Stark, *Eur. J. Med. Chem.*, 2014, **77**, 269–279.

38. E. Schmitt, G. Landelle, J.-P. Vors, N. Lui, S. Pazenok and F. R. Leroux, *Eur. J. Org. Chem.*, 2015, **2015**, 6052–6060.

39. L. Palatinus and G. Chapuis, *J. Appl. Crystallogr.*, 2007, **40**, 786–790.

40. G. M. Sheldrick, *Acta Crystallogr.*, 2008, **A64**, 112–122.

41. O. V. Dolomanov, L. J. Bourhis, R. J. Gildea, J. A. K. Howard and H. Puschmann, *J. Appl. Cryst.*, 2009, **42**, 339–341.

42. *CrysAlisPro, 1.171.36.20*; Agilent Technologies: Santa Clara, CA, 2012.

43. Y. Zhao and D. G. Truhlar, *Theor. Chem. Acc.*, 2007, **120**, 215–241.

44. Frisch, M. J.; Trucks, G. W.; Schlegel, H. B.; Scuseria, G. E.; Robb, M. A.; Cheeseman, J. R.; Scalmani, G.; Barone, V.; Mennucci, B.; Petersson, G. A.; Nakatsuji, H.; Caricato, M.; Li, X.; Hratchian, H. P.; Izmaylov, A. F.; Bloino, J.; Zheng, G.; Sonnenberg, J. L.; Hada, M.; Ehara, M.; Toyota, K.; Fukuda, R.; Hasegawa, J.; Ishida, M.; Nakajima, T.; Honda, Y.; Kitao, O.; Nakai, H.; Vreven, T.; Montgomery, J. A., Jr.; Peralta, J. E.; Ogliaro, F.; Bearpark, M.; Heyd, J. J.; Brothers, E.; Kudin, K. N.; Staroverov, V. N.; Keith, T.; Kobayashi, R.; Normand, J.; Raghavachari, K.; Rendell, A.; Burant, J. C.; Iyengar, S. S.; Tomasi, J.; Cossi, M.; Rega, N.; Millam, J. M.; Klene, M.; Knox, J. E.; Cross, J. B.; Bakken,

New Journal of Chemistry Accepted Manuscript

V.; Adamo, C.; Jaramillo, J.; Gomperts, R.; Stratmann, R. E.; Yazyev, O.; Austin, A. J.; Cammi, R.; Pomelli, C.; Ochterski, J. W.; Martin, R. L.; Morokuma, K.; Zakrzewski, V. G.; Voth, G. A.; Salvador, P.; Dannenberg, J. J.; Dapprich, S.; Daniels, A. D.; Farkas, O.; Foresman, J. B.; Ortiz, J. V.; Cioslowski, J.; Fox, D. J. *Gaussian 09*, Revision C.01; Gaussian, Inc.: Wallingford, CT, 2010.

45.   A. V. Marenich, C. J. Cramer and D. G. Truhlar, *J. Phys. Chem. B*, 2009, **113**, 6378–6396.

46.   T. Lu and F. Chen, *J. Comput. Chem.*, 2012, **33**, 580–592.

47.   E. D. Glendening, C. R. Landis and F. Weinhold, *WIREs Comput. Mol. Sci.*, 2012, **2**, 1–42.

New Journal of Chemistry Accepted Manuscript

27

TABLE OF CONTENTS
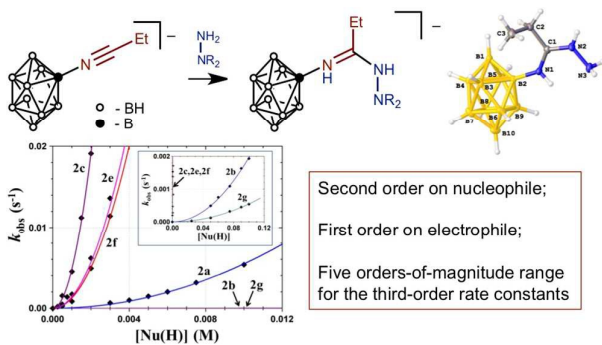
Three types of N(H)-nucleophiles were used to study the nucleophilic addition to the C≡N group of the 2-propanenitrilium *closo*-decaborate cluster giving *N-closo*-decaborato amidrazones. A nucleophilicity series for the N(H)-nucleophiles, with a range of structural types, has been obtained. The activation parameters for hydrazones indicate a small dependence on bond formation, but significantly negative entropies of activation with the latter contributing some 70–80% of the total Gibbs free energy of activation, $\Delta G^{\neq}$. In the X-ray structure of (*Z*)-(Ph$_3$PCH$_2$Ph)[**3g**], very rare intramolecular non-covalent interactions B–H•••π(Ph) were detected and studied theoretically.

New Journal of Chemistry Accepted Manuscript